Cell Reports
Methods

Article

Brain-wide circuit-specific targeting of astrocytes

Graphical abstract

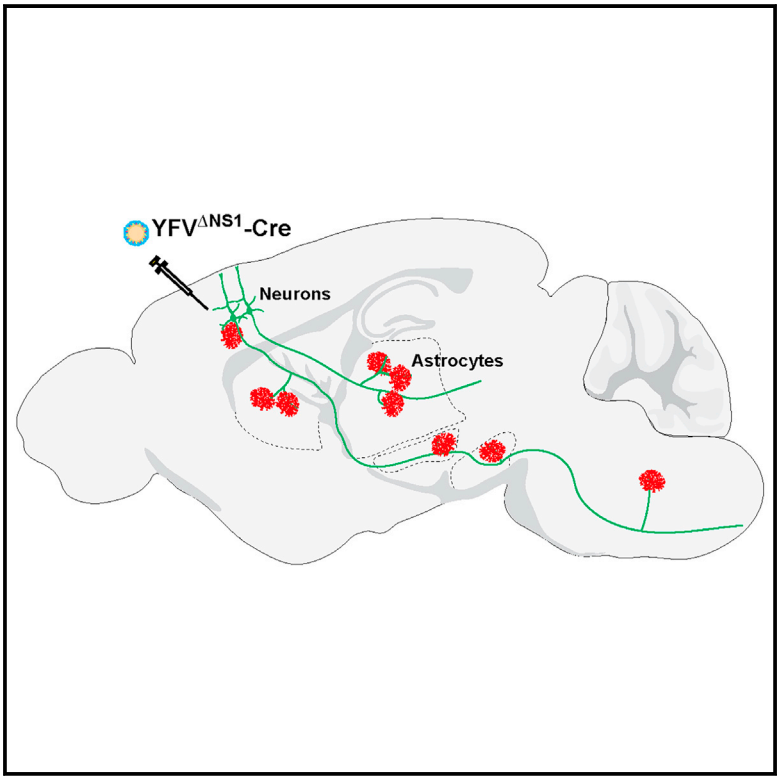

Authors

Alyssa Thompson, Rachel Arano, Uzair Saleem, ..., Yerim Kim, Ying Li, Wei Xu

Correspondence

ying1.li@utsouthwestern.edu (Y.L.), wei.xu1@utsouthwestern.edu (W.X.)

In brief

Astrocytes are heterogeneous and exert distinct functions in different neuronal circuits. However, selectively targeting circuit-specific astrocytes has been challenging. Here, Thompson et al. demonstrate that a viral vector based on the yellow fever vaccine can selectively turn on reporter genes in the astrocytes associated with specific neuronal projections.

Highlights

- Locally injected virus traces astrocytes at the whole-brain level
- Astrocyte tracing is neuronal circuit specific
- Restricted viral replication minimizes disturbance to astrocytes
- Tracing can be initiated from specific neuronal cell types

Thompson et al., 2023, Cell Reports Methods *3*, 100653
December 18, 2023
https://doi.org/10.1016/j.crmeth.2023.100653

CellPress

Cell Reports Methods

CellPress
OPEN ACCESS

Article

Brain-wide circuit-specific targeting of astrocytes

Alyssa Thompson,[1,2] Rachel Arano,[1,2] Uzair Saleem,[1] Rebecca Preciado,[1] Lizbeth Munoz,[1] Ian Nelson,[1] Katarina Ramos,[1] Yerim Kim,[1] Ying Li,[1,*] and Wei Xu[1,3,*]

[1]Department of Neuroscience, University of Texas Southwestern Medical Center, Dallas, TX 75390, USA
[2]These authors contributed equally
[3]Lead contact
*Correspondence: ying1.li@utsouthwestern.edu (Y.L.), wei.xu1@utsouthwestern.edu (W.X.)
https://doi.org/10.1016/j.crmeth.2023.100653

MOTIVATION Astrocytes, a major type of cells in the brain, are heterogeneous and have distinct functions in different circuits. Selective targeting of the astrocytes associated with specific neuronal circuits can enable investigation of circuit-specific roles. This study provides a tool for targeting circuit-specific astrocytes based on a transneuronal virus.

SUMMARY

Astrocytes are integral components of brain circuitry. They enwrap synapses, react to neuronal activity, and regulate synaptic transmission. Astrocytes are heterogeneous and exhibit distinct features and functions in different circuits. Selectively targeting the astrocytes associated with a given neuronal circuit would enable elucidation of their circuit-specific functions but has been technically challenging to date. Recently, we constructed anterograde transneuronal viral vectors based on yellow fever vaccine YFV-17D. Among them, the replication-incompetent YFV$^{\Delta NS1}$-Cre can selectively turn on reporter genes in postsynaptic neurons if the viral gene NS1 is expressed in postsynaptic neurons. Here we show that without exogenous expression of NS1 at the postsynaptic sites, locally injected YFV$^{\Delta NS1}$-Cre selectively turns on reporter genes in astrocytes in downstream brain regions. The targeting of astrocytes can occur across the whole brain but is specific for the neuronal circuits traced. Therefore, YFV$^{\Delta NS1}$-Cre provides a tool for selective genetic targeting of astrocytes to reveal their circuit-specific roles.

INTRODUCTION

Astrocytes are an essential component of synaptic communication besides providing physical and metabolic support to the neurons. Structurally, astrocytic processes contact or enwrap 50%–95% of the synapses in the brain to form tripartite synapses.[1,2] Developmentally, astrocytes contribute to synapse formation, maintenance, and plasticity. Synapses in the brain are formed primarily after astrogenesis; the molecules expressed or released from astrocytes determine synaptic features, regulate synapse maintenance, and determine the capacity for synaptic plasticity.[3–5] Functionally, astrocytes have bidirectional communication with neurons. They react to synaptic activities and in turn modulate synaptic or neuronal activities.[6–9] The impacts of astrocytes on synapses can be either highly localized through direct molecular or physiological interactions[10,11] or widespread by generation of calcium waves spreading across the astrocytic network.[12]

Astrocytes are heterogeneous and have circuit-specific functions.[11,13–15] Astrocytes, tiling the entire central nervous system, are one of the most abundant cell types in the brain. Despite the "even" distribution, astrocytes in different brain regions or circuits have distinct features in morphology, gene expression profiles, and reactions to signal molecules.[1,13,16,17] Consistent with the impacts of astrocytes on local synapses, astrocytes exert distinct influences on synapses in different circuits located in the same brain regions.[18–20] Therefore, astrocytes are functionally coupled to the synapses of specific neuronal circuits and play unique roles in these circuits.

Revealing the circuit-specific roles of astrocytes relies on technologies that target and control astrocytes in a circuit-specific manner. Research on astrocytes has been facilitated in recent years by the availability of genetic or viral tools to target astrocytes.[1,21] Combining these tools enables monitoring or manipulating astrocytes in a brain-region-specific manner. Recently, adeno-associated virus serotype 1 (AAV1) was shown to label astrocytes related to thalamus-cortex projections through axon-astrocyte transfer,[22] which represents a step forward for targeting circuit-specific astrocytes. However, AAV1 can spread in both anterograde and retrograde directions, which

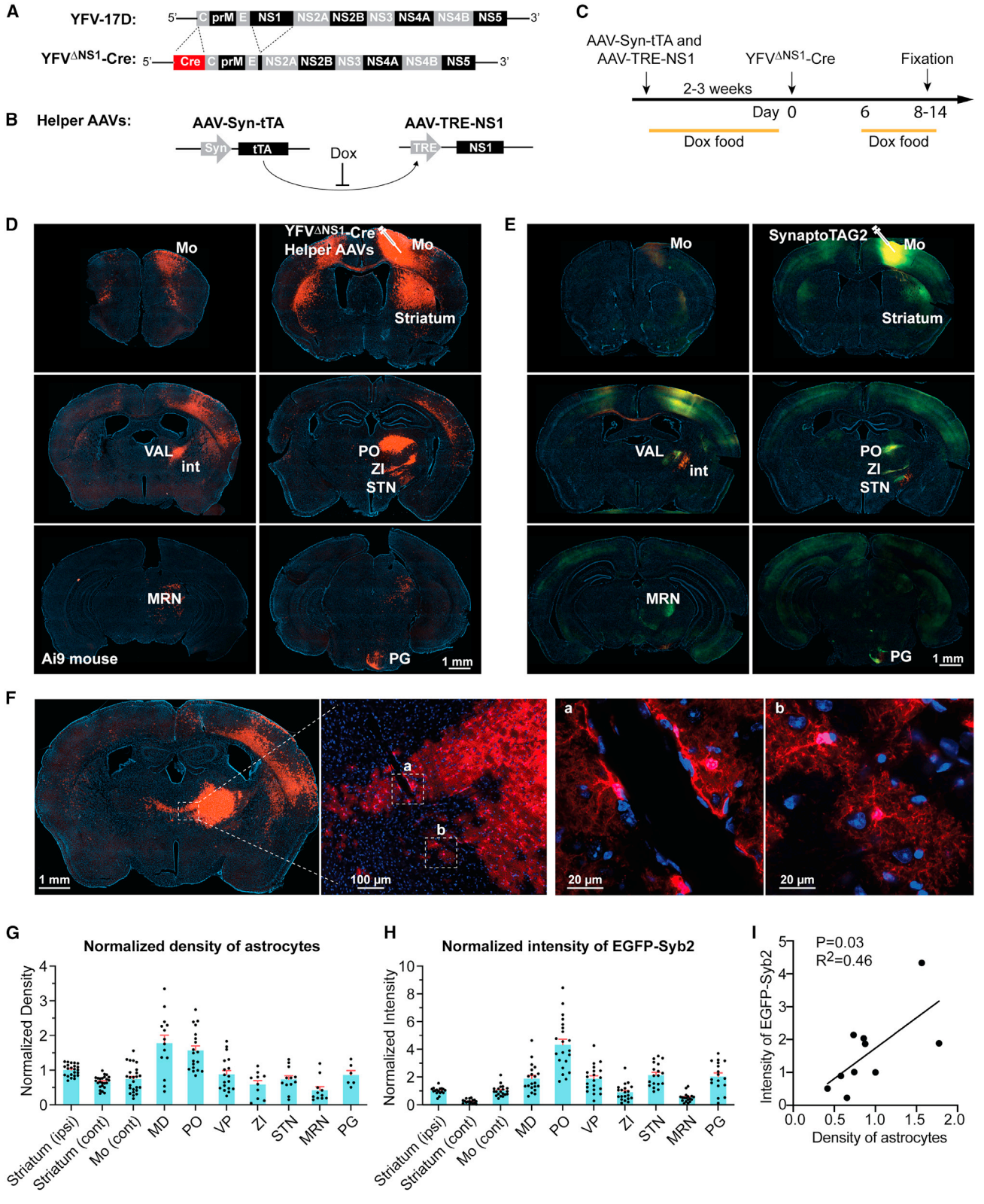

(legend on next page)

makes it difficult to determine the direction and route of spreading.[23–25] A generally applicable and efficient way to target circuit-specific astrocytes is still lacking.

We recently developed a transneuronal viral system based on a live attenuated vaccine for yellow fever that has been used in medicine since 1930s: YFV-17D.[26] YFV-17D is a positive-sense RNA virus. Its RNA genome encodes a polypeptide that is further cleaved into ten proteins. One of these proteins, NS1, is essential for the replication of YFV-17D. We previously constructed a replication-incompetent viral vector (YFV$^{\Delta NS1}$-Cre) by deleting NS1 and inserting Cre, a site-specific DNA recombinase, into the genome of YFV-17D (Figure 1A). YFV$^{\Delta NS1}$-Cre can spread to the postsynaptic neurons to turn on reporter genes if we exogenously express NS1 in postsynaptic neurons to enable replication of YFV$^{\Delta NS1}$-Cre. Surprisingly, here we find that in Cre reporter mouse lines, YFV$^{\Delta NS1}$-Cre, in the absence of postsynaptic expression of NS1, selectively turns on reporter genes in astrocytes in the postsynaptic sites. This therefore provides a technology to achieve circuit-specific genetic control of astrocytes.

RESULTS

Brain-wide targeting of astrocytes

We first examined the spreading of YFV$^{\Delta NS1}$-Cre in the brain of a Cre reporter mouse line, Ai9 mouse. Ai9 mouse carries the gene of red fluorescent protein tdTomato under a ubiquitous CAG promoter. A loxP-flanked STOP cassette inserted between the promoter and tdTomato coding sequence renders the expression of tdTomato in the presence of Cre.[27] We injected helper adeno-associated viruses (AAVs) into the primary motor cortex (Mo) of Ai9 mice to mediate the inducible expression of NS1; the AAVs are AAV-Syn-tTA (expression of tTA is driven by synapsin promoter) and AAV-TRE-NS1 (expression of NS1 is driven by Tet response element [TRE]) (Figure 1B). The inducible expression of NS1 allows us to control the timing of the replication of YFV$^{\Delta NS1}$-Cre: once YFV$^{\Delta NS1}$-Cre reaches the postsynaptic sites, we can turn off YFV$^{\Delta NS1}$-Cre replication in the starter neurons so that no extra virus is generated to harm cells. Because it takes time for the helper AAVs to infect neurons and express NS1 to a sufficient level to support the replication of YFV$^{\Delta NS1}$-Cre, we injected the AAVs 2 weeks before YFV$^{\Delta NS1}$-Cre. The mice ate food containing doxycycline (Dox) before and after the injections to restrict NS1 expression to a short time window (Figure 1C).[26] Two weeks later, we injected YFV$^{\Delta NS1}$-Cre into the same locus. NS1 expression allows YFV$^{\Delta NS1}$-Cre to replicate and spread to postsynaptic sites. 8–14 days later, we fixed the brains for histological analysis. In our previous work on YFV$^{\Delta NS1}$-Cre in combination with AAV reporter (e.g., AAV-Syn-DIO-jGCaMP7f), NS1 gene had to be expressed in the postsynaptic neurons to allow the reporter gene (e.g., jGCaMP7f) to turn on efficiently.[26] However, in Ai9 mice, without providing NS1 gene in the downstream regions, we observed a large number of cells expressing tdTomato throughout the brain (Figure 1D). These tdTomato-positive cells were found in brain regions known to be downstream targets of the motor cortex,[28] such as the contralateral cortex, the dorsal striatum, the nuclei in the thalamus, zona incerta, the subthalamic nucleus, the midbrain reticular nucleus, the pontine nucleus, and other brainstem structures. These cells were preferentially distributed in the hemisphere ipsilateral to the injection site.

At the viral injection site Mo, where NS1 was expressed, tdTomato-positive neurons were densely distributed together with cells lacking the typical morphology of neurons. Some of these tdTomato-positive cells expressed S100β, a marker for astrocytes (Figure S1). Outside the injection site, however, tdTomato-positive neurons were only sparsely observed in the brain regions receiving dense synaptic inputs from the Mo (such as the dorsal striatum) and were barely detectable in other brain regions. Most of the tdTomato-positive cells had the typical morphology of protoplasmic astrocytes characterized by a highly branched bushy arborization (Figures 1D–1F).[29–32] Sometimes these processes lined up the walls of the brain blood vessels in endfoot-like structures (Figure 1F), another feature of astrocytes.[33] These results indicate that YFV$^{\Delta NS1}$-Cre can infect astrocytes associated with specific synaptic projections at the whole-brain level.

To further examine the relationship between the distribution patterns of these tdTomato-positive cells and motor cortex synaptic projections, we injected SynaptoTAG2 AAV into the motor cortex. SynaptoTAG2 expresses tdTomato to mark the infected

Figure 1. Locally injected YFV$^{\Delta NS1}$-Cre turns on reporter gene in astrocytes at whole-brain level

(A) Schematics showing the RNA genomes of YFV-17D and YFV$^{\Delta NS1}$-Cre.

(B) Schematics showing the two helper AAVs for controlling the replication of YFV$^{\Delta NS1}$-Cre.

(C) The experimental procedures. Mice ate food containing doxycycline (Dox) except from 2 days before to 6 days after injection of YFV$^{\Delta NS1}$-Cre so that NS1 was expressed only during the 8 days to allow YFV$^{\Delta NS1}$-Cre to replicate.

(D) Expression of tdTomato (red) in the brain after injection of YFV$^{\Delta NS1}$-Cre into the motor cortex (Mo) of Ai9 mouse. The helper AAVs were AAV-Syn-tTA and AAV-TRE-NS1. Blue shows counterstaining with DAPI.

(E) Axonal and synaptic projections traced by SynaptoTAG2 AAV from Mo.

(F) High-resolution photos of the tdTomato-positive cells traced from the Mo by YFV$^{\Delta NS1}$-Cre. The two photos on the right are high-resolution views of the indicated areas in the second photo from the left.

(G) Density of tdTomato-positive astrocytes in each indicated brain region, normalized to that of the ipsilateral striatum. Data are presented as scatterplot showing density measured from each brain image and bar graph showing mean + standard error of the mean (SEM). n = 6–25 images from five mice.

(H) Intensity of green fluorescence of EGFP-syb2 (in SynaptoTAG2) in each indicated brain region, normalized to that of the ipsilateral striatum. Data are presented as scatterplot showing intensity measured from each brain image and bar graph showing mean + SEM. n = 17–21 images from five mice.

(I) Correlation between the averaged density of tdTomato-positive astrocytes and the intensity of EGFP-Syb2 in the brain regions listed in (G) and (H).

VAL, ventral anterior-lateral complex of the thalamus; MD, medial dorsal nucleus of thalamus; PO, posterior complex of the thalamus; VP, ventral posterior complex of the thalamus; ZI, zona incerta; STN, subthalamic nucleus; int, internal capsule; MRN, midbrain reticular nucleus; PG, pontine gray; ipsi, ipsilateral; cont, contralateral.

See also Figure S1.

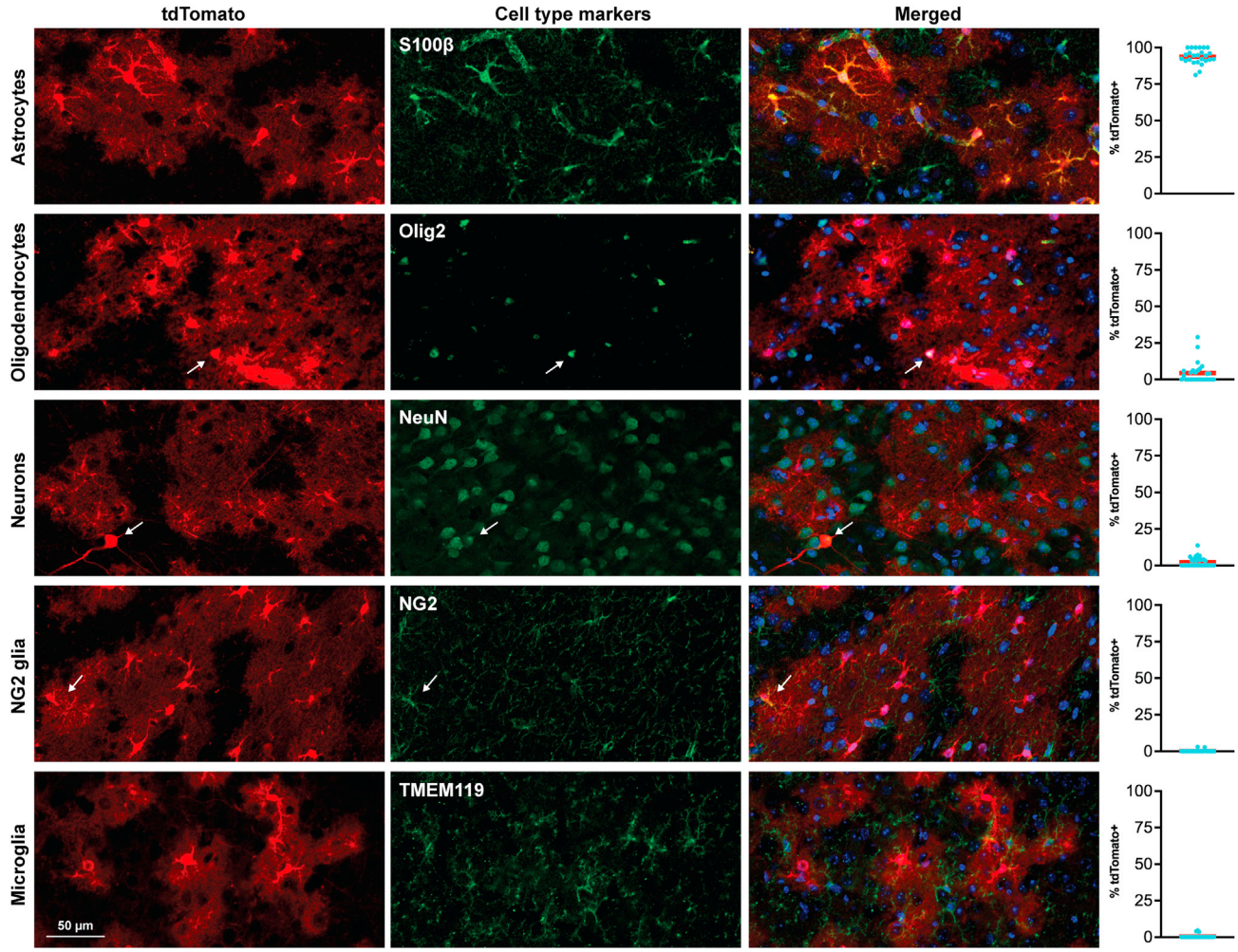

Figure 2. YFV$^{\Delta NS1}$-Cre turns on reporter gene in astrocytes

Immunohistochemistry of the brain sections from mice with YFV$^{\Delta NS1}$-Cre injected into the motor cortex with antibodies for the markers of different cell types, including S100β for astrocytes, Olig2 for oligodendrocytes, NeuN for neurons, NG2 for NG2 glia (oligodendrocyte precursor cells), and TMEM119 for microglia. Blue shows counterstaining with DAPI. Arrows indicate the tdTomato-positive cells labeled by immunostaining of cell-type markers. Scatterplots show quantification of the percentage of tdTomato-positive cells that were immunoreactive to respective antibodies. Each blue dot represents the measurement from one image. Red bars are the means. n = 25–31 images from three mice (for each mouse, 2–4 images were collected from each of the three brain regions: the striatum, the thalamus, and the contralateral motor cortex).

See also Figures S2 and S3.

neurons and expresses EGFP fused with synaptobrevin-2 (EGFP-Syb2) to label synaptic terminals.[26] The EGFP signal was present in the same brain regions as those of tdTomato-positive cells in Ai9 mice (Figure 1E). We counted the number of tdTomato-positive astrocytes (traced with YFV$^{\Delta NS1}$-Cre) in each of the downstream brain regions and calculated the average density by dividing the cell number by the area of the brain region. These average densities positively correlate with the average green fluorescence intensities of EGFP-Syb2 (traced with SynaptoTAG2) in the corresponding brain regions (Figures 1G–1I). Moreover, these tdTomato-positive cells were present in the regions receiving synaptic inputs from motor cortex (marked by EGFP) but were rarely found in regions with axonal bundles only (e.g., internal capsule in Figure 1D), suggesting that YFV$^{\Delta NS1}$-Cre primarily infected cells associated with synaptic terminals originating from the injection site.

Selective targeting of astrocytes

We conducted immunohistochemistry with antibodies of the markers for the major brain cell types to confirm the identities of these tdTomato-positive cells in Ai9 mice (Figure 2). As expected, outside the injection site only a small fraction (2.24%) of these cells was positive for NeuN, a neuronal marker, and they were mainly in the striatum. In other brain regions NeuN was barely detected in the tdTomato-positive cells. On average, 93.7% of the cells were positive for S100β. Some tdTomato-positive cells (4.38%) were positive for Olig2, indicating that they were oligodendrocytes. These oligodendrocytes were mainly

CellPress
OPEN ACCESS

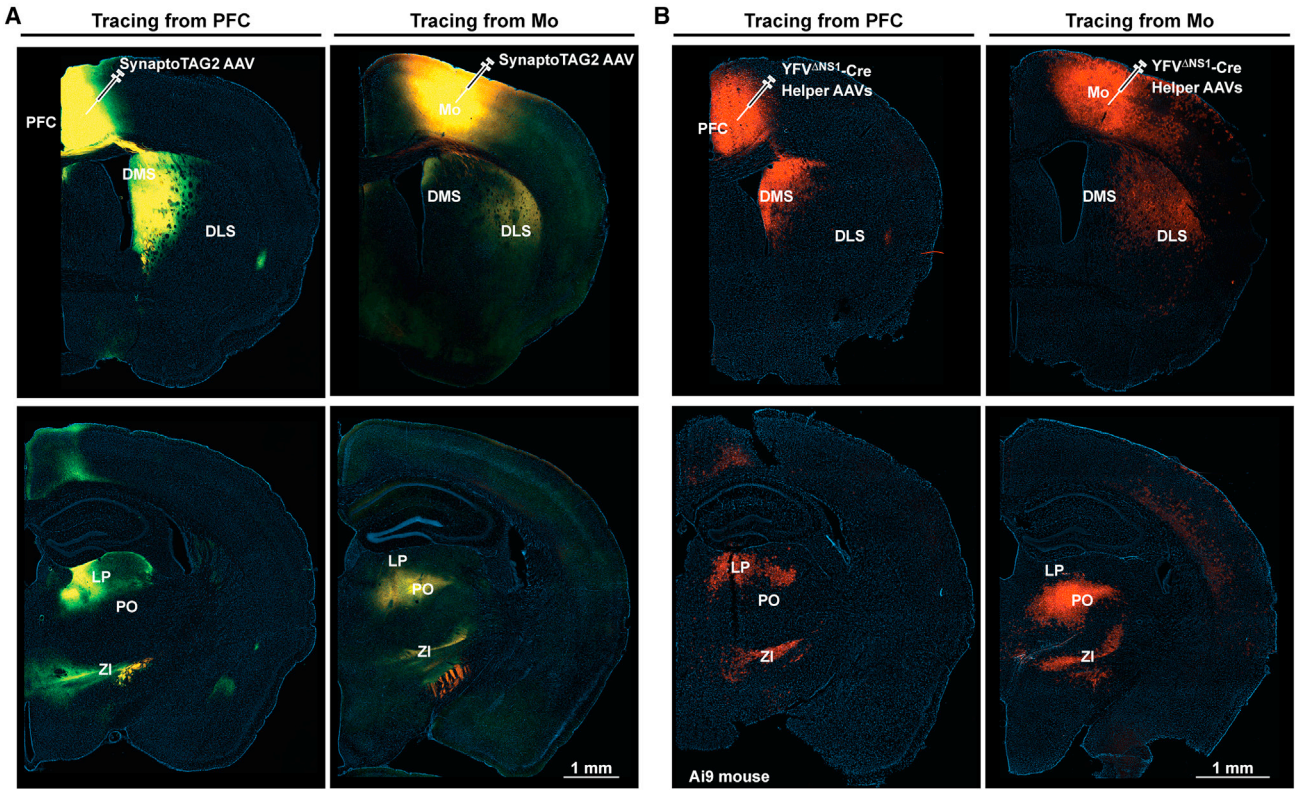

Figure 3. YFV$^{\Delta NS1}$-Cre traces the astrocytes in two corticofugal pathways

(A) Synaptic projections traced by SynaptoTAG2 AAV from the PFC or motor cortex (Mo) to different areas in the striatum and thalamus. When SynaptoTAG2 AAV was injected into the PFC, green fluorescence was observed in the dorsomedial striatum (DMS), the lateral posterior nucleus (LP), and zona incerta (ZI). When SynaptoTAG2 AAV was injected into the Mo, green fluorescence was observed in the dorsolateral striatum (DLS), posterior complex of the thalamus (PO), and ZI.

(B) Traced astrocytes in corticofugal pathways originating from the PFC or Mo with YFV$^{\Delta NS1}$-Cre in Ai9 mice.

The experiments were performed in three (A, left), four (A, right), three (B, left), and five (B, right) mice, respectively, and similar results were obtained.

See also Figure S4.

located in the corpus callosum or axonal bundles in gray matter. Few tdTomato-positive cells were positive for NG2 (0.21%), a marker for oligodendrocyte precursor cells, or TMEM119 (0.47%), a marker for microglia. These results indicate that with the exception of a small fraction of neurons (in the heavily innervated regions) or oligodendrocytes (in axonal bundles), YFV$^{\Delta NS1}$-Cre selectively targets astrocytes in the downstream regions in the absence of NS1.

We also examined the percentage of S100β-positive astrocytes that were tdTomato-positive in the brain regions downstream of the Mo. In the posterior complex (PO) of the thalamus ipsilateral to viral injection site, on average 60.6% of S100β-positive astrocytes were positive for tdTomato; in the dorsolateral striatum and midbrain reticular nucleus (MRN) regions the percentages were 40.1% and 14.0%, respectively (Figure S2). These results are consistent with those in Figure 1, suggesting that the fraction of astrocytes traced correlate with the level of synaptic innervation from the starter neurons.

This preferential infection of astrocytes is in sharp contrast to many other versions of the viral vectors derived from YFV-17D. For comparison, we tested in the Mo YFV$^{\Delta CME}$-mVenus, a packaging-deficient version of YFV-17D we made to trace neuronal connections (Figure S3).[26] Similar to our previous observations, we detected mVenus-positive cells in the brain regions downstream of the Mo (Figure S3A). These mVenus-positive cells had typical neuronal morphology (Figure S3B) and were barely co-labeled with S100β (Figure S3C). These results indicate that with different experimental designs, these YFV-17D derived viral vectors can be used to trace either neurons or astrocytes associated with the starter neurons; and in both scenarios, a high level of selectivity (for either neurons or astrocytes) can be achieved.

Input specificity of astrocyte targeting

We next investigated whether the astrocytes labeled by YFV$^{\Delta NS1}$-Cre were specific to the neuronal circuits. Unlike the neuron-neuron connections that can be analyzed with electrophysiology, we compared the astrocytes traced from two adjacent brain regions to find out whether the labeling was confined to their respective downstream regions (Figures 3, 4, S4, and S5).

We first compared tracing from the prefrontal cortex (PFC) with that from the motor cortex (Mo). These two cortical regions selectively project to two distinct anatomical domains of the

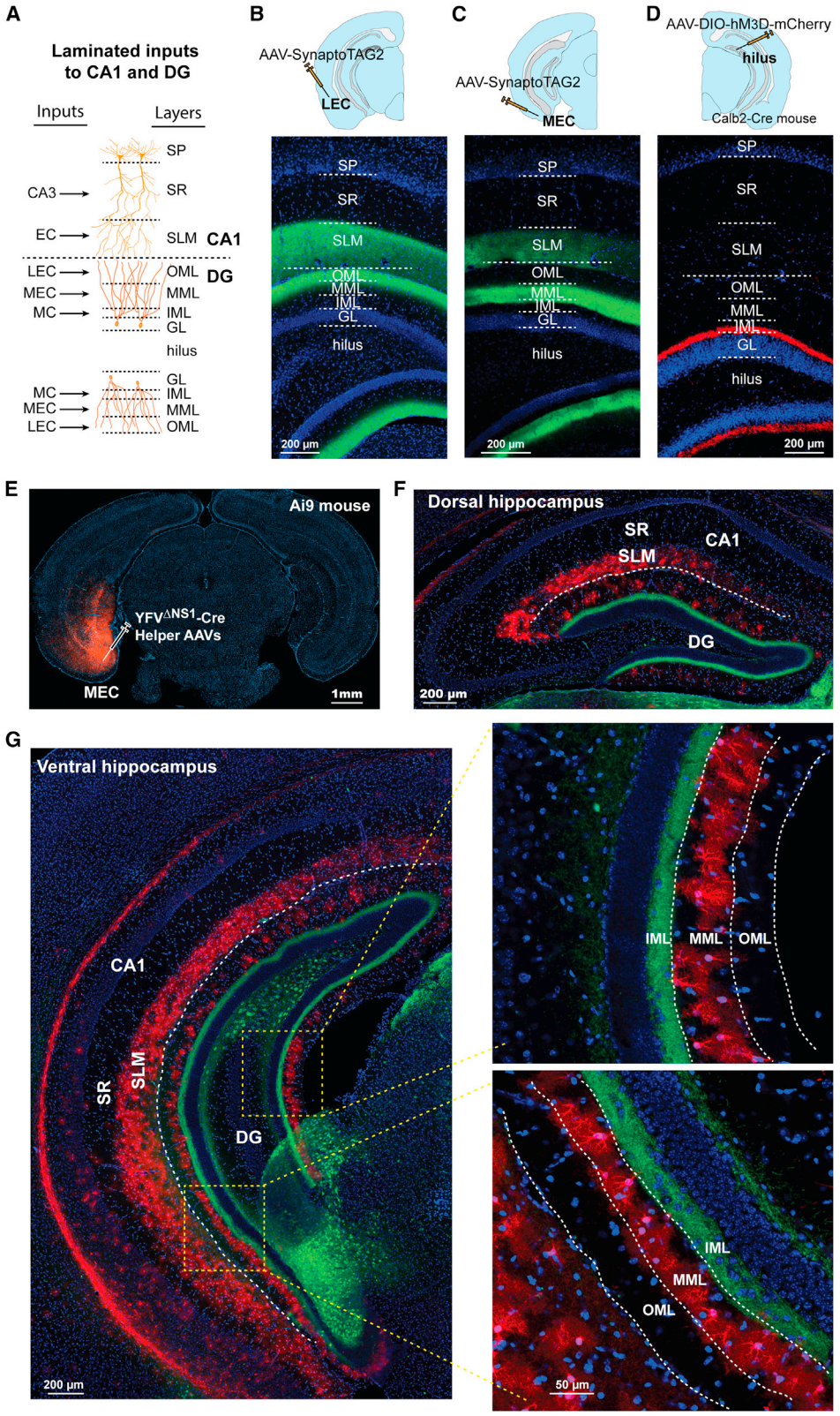

(legend on next page)

dorsal striatum, the dorsomedial striatum (DMS) and the dorsolateral striatum (DLS), to regulate distinct behavioral modes, respectively.[34] Similarly, PFC and Mo differentially innervate two adjacent thalamic regions, the lateral posterior nucleus (LP) and posterior complex (PO), respectively. These innervation patterns were recaptured by tracing with SynaptoTAG2 AAV (Figure 3A). We injected helper AAVs (AAV-Syn-tTA and AAV-TRE-NS1) and later YFV$^{\Delta NS1}$-Cre into the PFC or Mo, respectively. In the striatum, the tdTomato-positive astrocytes were observed primarily in the DMS when YFV$^{\Delta NS1}$-Cre was injected into the PFC, whereas they were in the DLS when YFV$^{\Delta NS1}$-Cre was injected into the Mo (Figures 3B and S4). Similarly, in the dorsal thalamus, the traced astrocytes were in the LP when YFV$^{\Delta NS1}$-Cre was injected into the PFC but in PO when YFV$^{\Delta NS1}$-Cre was injected into the Mo, suggesting that YFV$^{\Delta NS1}$-Cre only infected astrocytes associated with the neuronal circuits they traced.

We also checked the circuits from the entorhinal cortex to the hippocampus. The inputs from the entorhinal cortex to the hippocampus are arranged in a highly laminated fashion (Figure 4A). In the CA1 region of the hippocampus, the entorhinal neurons send inputs to stratum lacunosum moleculare (SLM) to innervate the distal dendrites of the CA1 pyramidal cells and avoid the stratum radiatum (SR), where the proximal dendrites of pyramidal cells reside. In the dentate gyrus (DG), the molecular layer receives a majority of synaptic inputs from the entorhinal cortex and mossy cells. The molecular layer can be further divided into the outer, middle, and inner molecular layers (OML, MML, and IML), which receive synaptic inputs from the lateral entorhinal cortex (LEC), medial entorhinal cortex (MEC), and the mossy cells, respectively. These innervation patterns can be recaptured by SynaptoTAG2 tracing from LEC or MEC (Figures 4B and 4C) or by injecting Cre-dependent AAV into calbindin-2 Cre mouse (calbindin-2 is expressed by mossy cells) (Figure 4D).

We studied the astrocytes traced from LEC or MEC, respectively. When YFV$^{\Delta NS1}$-Cre was injected to the MEC, the labeled astrocytes were mainly distributed in the MML (Figures 4E–4G). Within the MML, especially the MML of the ventral hippocampus, a single layer of astrocytes was labeled, suggesting a high level of circuit specificity. Similarly, when YFV$^{\Delta NS1}$-Cre was injected into the LEC, the labeled astrocytes were mainly in the OML (Figure S4). These results further demonstrate that the labeled astrocytes are associated with the traced neuronal circuits.

We further examined whether YFV$^{\Delta NS1}$-Cre worked with other mouse lines. We conducted the same viral injections in Ai6 mice that express the GFP ZSGeen1 upon the expression of Cre. Similarly, we observed labeling of astrocytes in the regions receiving synaptic inputs from the viral injection site (Figures S5A and S5B), suggesting that YFV$^{\Delta NS1}$-Cre could turn on Cre-dependent gene expression in different mouse lines. We also tested whether YFV$^{\Delta NS1}$-Cre could turn on reporter genes carried by AAVs. We generated AAV5 expressing hM3Dq fused with mCherry under the control of an astrocyte-specific GfaABC1D promoter and injected it into the striatum. To our disappointment, we barely detected mCherry-positive astrocytes (Figures S5C and S5D). The results indicate that YFV$^{\Delta NS1}$-Cre cannot efficiently turn on an AAV reporter in the postsynaptic brain regions. A possible reason for this is that the AAV infection triggers the defense mechanisms of astrocytes, which makes these astrocytes resistant to YFV-17D infection. In a recent study, AAV1-Cre was shown to trace astrocytes associated with a neuronal projection.[22] Consistent with this finding, we found that when AAV1-Cre was injected into the MEC of Ai9 mice, the astrocytes in the MML became positive for tdTomato (Figure S5E) while a large number of granule cells were also tdTomato positive, indicating that AAV1-Cre traced both neurons and astrocytes and that AAV1-Cre may need to be combined with local injection of AAV carrying an astrocyte-specific promoter to selectively target astrocytes.

Tracing astrocytes from specific types of neurons

The brain has numerous neuronal cell types. Each type shows a specific morphology, connectivity, and activity pattern. Since the replication and transneuronal spreading of YFV$^{\Delta NS1}$-Cre can be controlled by inducible expression of NS1, we tested whether we could trace the astrocytes associated with the synaptic projections from different neuronal cell types. We generated AAV vectors to express tTA under either CamK2 promoter or Dlx promoter, which drives gene expression selectively in the forebrain glutamatergic or GABAergic neurons, respectively.[35] We tested these AAVs, in combination with YFV$^{\Delta NS1}$-Cre, in the lateral septum (LS), a brain region that is composed of predominantly GABAergic neurons.[36] Glutamatergic neurons were barely detected in the dorsal part of the LS where we injected the viruses.[37] We first injected into the LS AAV-Dlx-SynaptoTAG, which traced the axonal and synaptic projections of GABAergic neurons.[38] Similar to previous reports, the most prominent downstream targets of LS are medial septum, diagonal band nucleus (NDB), lateral hypothalamus, and the CA3 region of the hippocampus (Figures 5A and 5D). In Ai9 mice when we used AAV-Dlx-tTA to induce the expression of NS1 to *trans*-complement YFV$^{\Delta NS1}$-Cre, we detected

Figure 4. Input-specific tracing of astrocytes in entorhinal cortex-hippocampus circuits

(A) Schematics showing that three streams of axonal inputs, from lateral entorhinal cortex (LEC), medial entorhinal cortex (MEC), and mossy cells (MC), form synapses at different layers in the CA1 and dentate gyrus (DG). SP, stratum pyramidale; SR, stratum radiatum; SLM, stratum lacunosum moleculare; OML/MML/IML, outer/middle/inner molecular layer; GL, granule cell layer.

(B and C) Tracing with SynaptoTAG2 AAVs from the LEC (B) or MEC (C), respectively.

(D) Tracing axonal projection of mossy cells.

(E–G) Tracing astrocytes by injecting YFV$^{\Delta NS1}$-Cre into the MEC in an Ai9 mouse. Brain sections were immunostained with Calb2 (green) to outline the IML. Blue shows counterstaining with DAPI. White dashed lines indicate the border between the CA1 and DG or the borders between OML, MML, and IML.

Each of the experiments shown in (B)–(D) and (E)–(G) were performed in three mice, and similar results were obtained.

See also Figures S4 and S5.

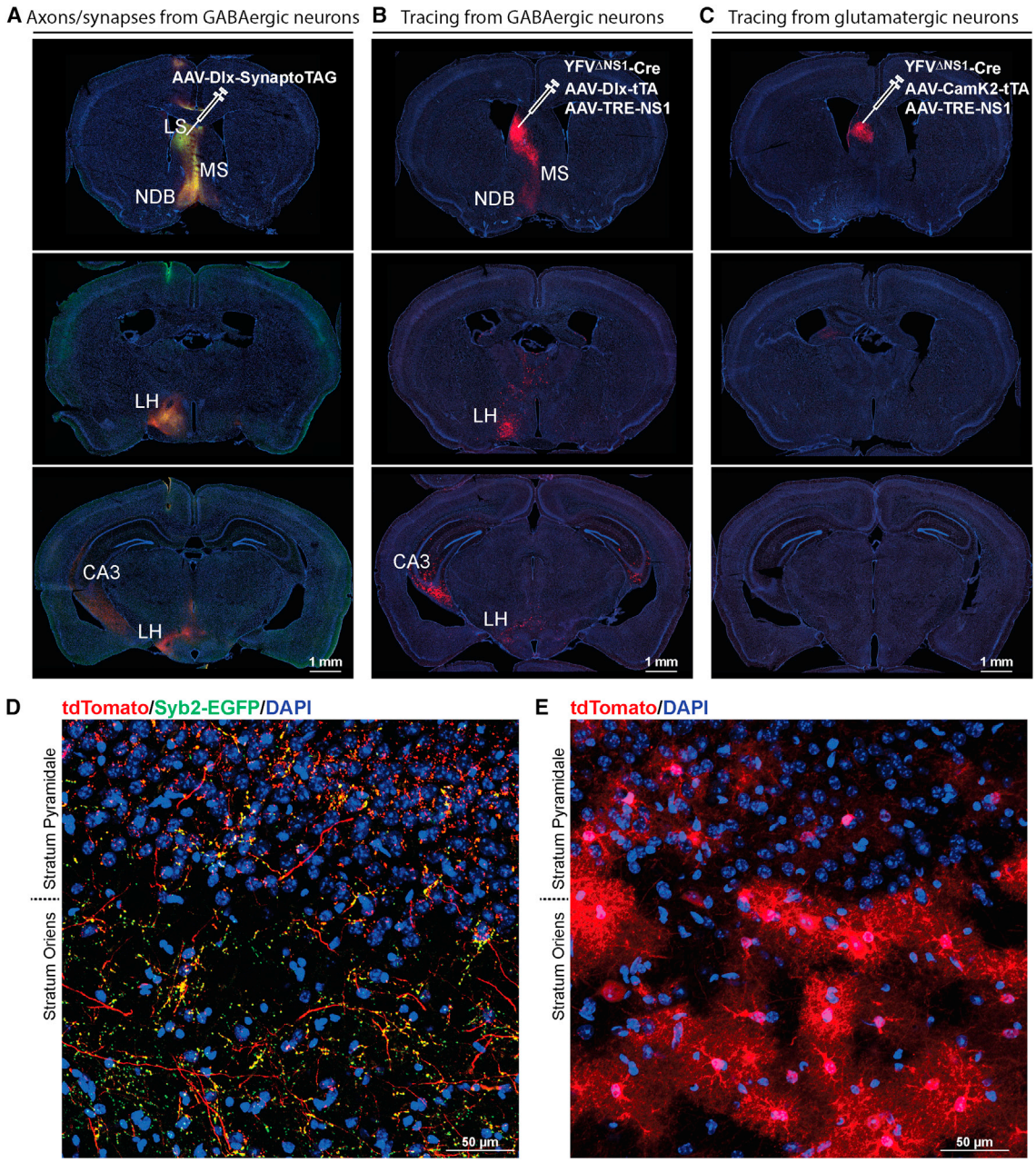

Figure 5. Tracing astrocytes from specific neuronal cell types

(A) Tracing synaptic projections from GABAergic neurons in lateral septum (LS) with AAV-Dlx-SynaptoTAG.

(B) Tracing astrocytes with YFV$^{\Delta NS1}$-Cre from GABAergic neurons in LS in Ai9 mice. The helper AAVs, AAV-Dlx-tTA and AAV-TRE-NS1, were used to express NS1 selectively in GABAergic neurons.

(C) Tracing astrocytes with YFV$^{\Delta NS1}$-Cre from glutamatergic neurons in LS in Ai9 mice.

(D) High-resolution image of the CA3 region shown in (A).

(E) High-resolution image of the CA3 region shown in (B).

LS, lateral septum; MS, medial septum; NDB, nucleus of the diagonal band; LH, lateral hypothalamus.

See also Figure S6.

tdTomato-positive astrocytes in the major synaptic targets of the LS (Figures 5B and 5E). Conversely, when we used AAV-CamK2-tTA to induce NS1 expression in glutamatergic neurons in the LS, tdTomato-positive astrocytes (and neurons) were mainly confined to the injection sites (Figure 5C). These local astrocytes were likely directly infected by the injected YFV$^{\Delta NS1}$-Cre but not by those transneuronally transported YFV$^{\Delta NS1}$-Cre. We then tested the AAV-CamK2-tTA in the Mo,

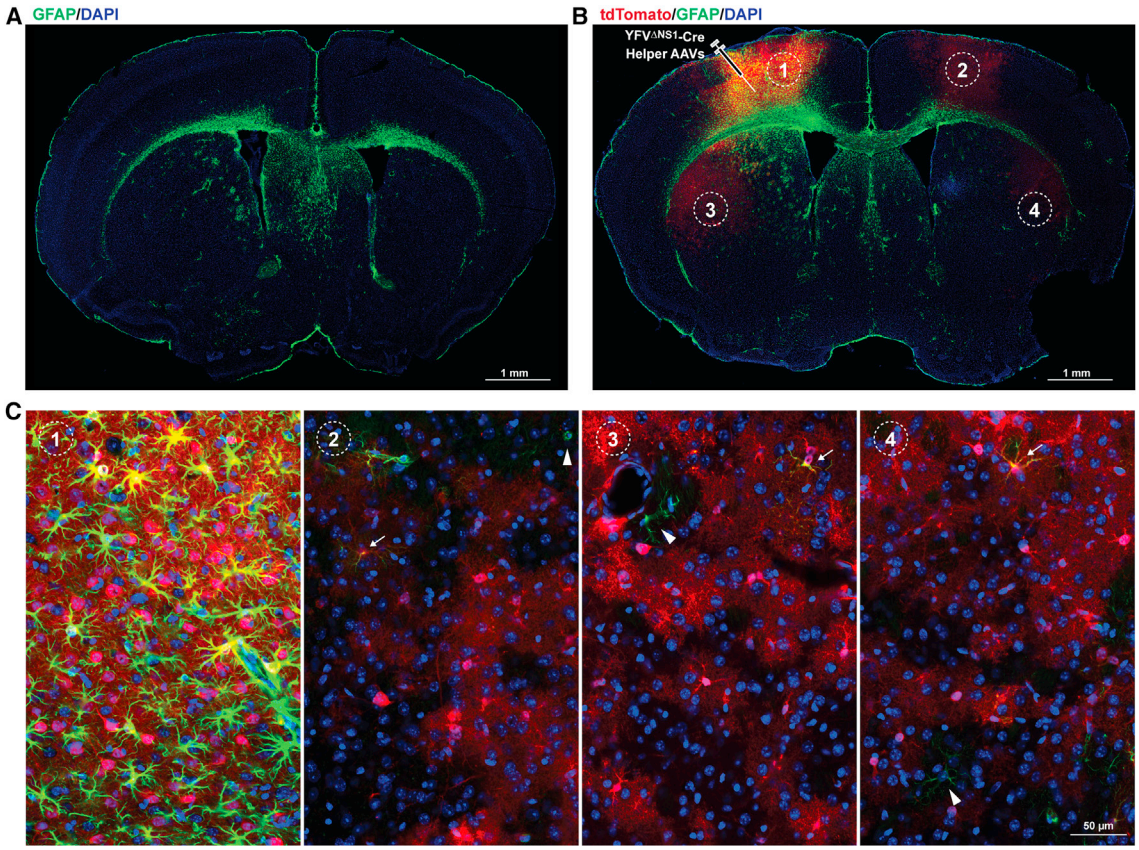

Figure 6. Reactive astrocytes in mice receiving viral injections

(A) Immunostaining of GFAP in a mouse receiving no viral injection.

(B) Expression of GFAP in Ai9 mouse receiving injections of helper AAVs (AAV-Syn-tTA and AAV-TRE-NS1) and YFV$^{\Delta NS1}$-Cre.

(C) High-resolution confocal images of the regions indicated by the numbers in circles in (B).

See also Figure S7.

a brain region rich in glutamatergic neurons. We detected tdTomato-positive astrocytes in the downstream regions of the Mo (Figure S6). These results indicate that by controlling NS1 expression in specific neuronal cell types, we can trace the astrocytes associated with the synaptic projections from these cell types.

Impacts of viral infection on astrocytes

Astrocytes are sensitive to local damage or infection.[39] It is important to know whether viral infection and viral replication trigger astrogliosis or alter astrocyte functions. Here we conducted immunostaining of glial fibrillary acidic protein (GFAP) as a way to monitor astrocyte reactivity. We injected helper AAVs (AAV-Syn-tTA and AAV-TRE-NS1) and YFV$^{\Delta NS1}$-Cre into the Mo sequentially, fixed the brain with the same protocol described above, and stained the sections for GFAP expression. In most brain regions (including the cortex and striatum, thalamus) of intact mice that were not injected with viruses, the majority of cells had a low level of GFAP expression, albeit there were some scattered cells with high-level GFAP expression (Figures 6A and S7). In the brains injected with the helper AAVs (AAV-Syn-tTA and AAV-TRE-NS1) and YFV$^{\Delta NS1}$-Cre, GFAP expression increased at the injection site (Figures 6B, 6C, and S7D). These reactive astrocytes may be caused by local damage introduced through stereotactic injection; the infections by AAVs,[40] and/or the infection by YFV$^{\Delta NS1}$-Cre. GFAP expression also increased in the region adjacent to the injection site, where no or few tdTomato-positive cells were present (Figure S7F), suggesting that at least in this area, the reactive astrocytes might not be induced by the infection of YFV$^{\Delta NS1}$-Cre. In the brain regions downstream of the Mo, GFAP expression did not increase. In these downstream regions, we compared the intensity of GFAP immunostaining in the areas covered by tdTomato-positive astrocyte processes and the areas in the same images that were not covered by tdTomato-positive astrocytes, and found no difference (Figure S7E), indicating that YFV$^{\Delta NS1}$-Cre infection did not lead to reactive astrocytes in these downstream areas that received synaptic innervation from the injection site (the Mo).

DISCUSSION

While we have gained tremendous knowledge of brain circuitry in recent years thanks to the technologies for selectively

targeting neurons in different circuits, we are just beginning to uncover the circuit-specific roles that astrocytes play, partly due to the lack of tools. In line with their roles in synaptic transmission, cognition, and emotion,[41,42] astrocytes are also critically involved in the pathogenesis of multiple brain disorders, such as amyotrophic lateral sclerosis (ALS), Alzheimer's disease, autism spectrum disorder, and epilepsy.[43–47] The astrocytes involved in a disorder may be located in various regions but associated with a specific circuit (e.g., motor cortex-spinal cord circuit in ALS). The lack of technology to target astrocytes in a pathway-specific manner has also impeded the development of effective therapies. Therefore, the brain-wide circuit-specific targeting of astrocytes can be tools for in-depth analysis of astrocyte functions and has the potential to be developed into treatments for brain disorders.

Preferential targeting of astrocytes

We previously used replication-capable YFV-17D vectors (YFV-mVenus) or the replication-incompetent vectors (YFV$^{\Delta NS1}$-mVenus or YFV$^{\Delta NS1}$-Cre) to track neuronal projections.[26] In these experiments, neurons were almost exclusively labeled, similarly to YFV$^{\Delta CME}$-mVenus tracing in Figure S3. For the replication-incompetent versions, we had to express NS1 in the postsynaptic neurons; otherwise, the labeling would be very sparse (for YFV$^{\Delta NS1}$-Cre) or not detectable (for YFV$^{\Delta NS1}$-mVenus). Why does YFV$^{\Delta NS1}$-Cre label almost exclusively astrocytes in the brain regions downstream of the injection site in the reporter mice? These results clearly demonstrate that YFV-17D can infect astrocytes. The lack of labeling of astrocytes by the replication-capable YFV-mVenus therefore suggests that YFV-17D cannot effectively replicate its genome in astrocytes to generate fluorescent proteins at a detectable level. Without replication, the small number of RNA viral genomes in a cell may soon degrade and will not be able to sustain the expression of fluorescent proteins. The lack of effective replication in astrocytes could be due to the antiviral machinery in astrocytes as shown in other flaviviruses.[48] In the case of YFV$^{\Delta NS1}$-Cre, transient expression of Cre may be enough to turn on the permanent expression of a reporter gene. How, then, does YFV$^{\Delta NS1}$-Cre effectively label astrocytes instead of neurons in the absence of NS1? An astrocyte is frequently associated with 100,000 synapses, about ten times more than that of most neurons.[49] Therefore, astrocytes, compared to neurons in the same pathway, may collect more copies of YFV$^{\Delta NS1}$-Cre from the presynaptic neurons, which in turn express Cre to a sufficient level to turn on the reporter gene without viral replication. In our early study with NS1 expressed in postsynaptic neurons, the reporter gene was under a neuronal promoter, hence YFV$^{\Delta NS1}$-Cre labeled only neurons. Therefore, by adjusting the experimental configurations, YFV$^{\Delta NS1}$-Cre can be used to analyze either neuronal projections or circuit-specific astrocytes (Figure 7).

Trans-synaptic spreading vs. spreading by "accessible" proximity

For decades, viruses have been used to map neuron-to-neuron connectivity. Despite the proven value of these tools, their exact routes and mechanisms of spreading in the brain remain unclear. On one hand, many viruses, especially rabies virus that has been the most used and characterized, show a high fidelity in tracking the synaptically connected neurons.[50,51] This level of specificity apparently cannot be explained by simple diffusion of virions in brain tissue. On the other hand, we lack strong evidence supporting that the viral spreading relies on structures or proteins specific to synapses. In fact, in addition to YFV-17D, many "tracer" viruses, including rabies virus,[52,53] pseudorabies virus,[54] and herpes simplex virus type 1 (HSV 1),[55–57] infect glial cells. The majority of these glial cells may not form synapses with neurons. How can we reconcile these findings? One possibility is that the viruses indeed spread by "proximity" as argued by many researchers[58]; however, this "proximity" is not just a short distance between axons and postsynaptic sites; instead, it emphasizes the accessibility of the axons to the postsynaptic sites. Most of the surfaces of the neurons, including axons and dendrites, are in close contact with glial cells. If the glial cells are infected but do not support the replication and release of new viral particles, they restrict viral spreading between connected neurons.[59] Our data here support this restrictive role of astrocytes in the spreading of YFV-17D vectors.

Advantages, limitations, and future improvements

This viral tool has a few advantages. First, it selectively targets astrocytes in the postsynaptic regions. Using YFV$^{\Delta NS1}$-Cre in reporter mouse lines expressing fluorescent proteins or calcium indicators,[60] we can examine the morphological or activity features of the circuit-specific astrocytes. We can also prelabel the astrocytes in a specific pathway to monitor their migration or morphological plasticity when their associated neuronal projections are subjected to functional alterations or pathological damage. Using it in reporter mice expressing effector proteins, such as DREADDs or channelrhodopsin,[61] we can selectively stimulate or silence these astrocytes with high temporal and spatial precision. We can also use them in various conditional knockout lines to determine the contributions of astrocytic genes to synapse formation or synaptic functions.[4] Second, the tracing of astrocytes is at the whole-brain level. It allows us to examine the astrocytes in many brain regions, albeit associated with the same starter neurons, simultaneously in the same animals. Third, the presence of YFV$^{\Delta NS1}$-Cre in astrocytes is transient. RNAs in live cells have short life spans. Without replication, YFV$^{\Delta NS1}$-Cre RNA genome in traced astrocytes degrades soon after infection and leaves minimal long-term impacts except turning on the intended reporter genes. In the downstream brain regions, without local surgical damage or AAV infection, astrogliosis or other functional disturbances of astrocytes are minimized, making it ideal for studying the roles of astrocytes in diseases. Furthermore, YFV$^{\Delta NS1}$-Cre can trace astrocytes associated with specific presynaptic neuronal cell types when we restrict its replication to the particular neuronal type. With these advantages, this tool can reveal circuit-specific roles of astrocytes.

Limitations of study

First, the surgery involves two sequential injections that require accurate targeting in stereotaxic injections to ensure that these two injections are in the same brain region. We may be able to

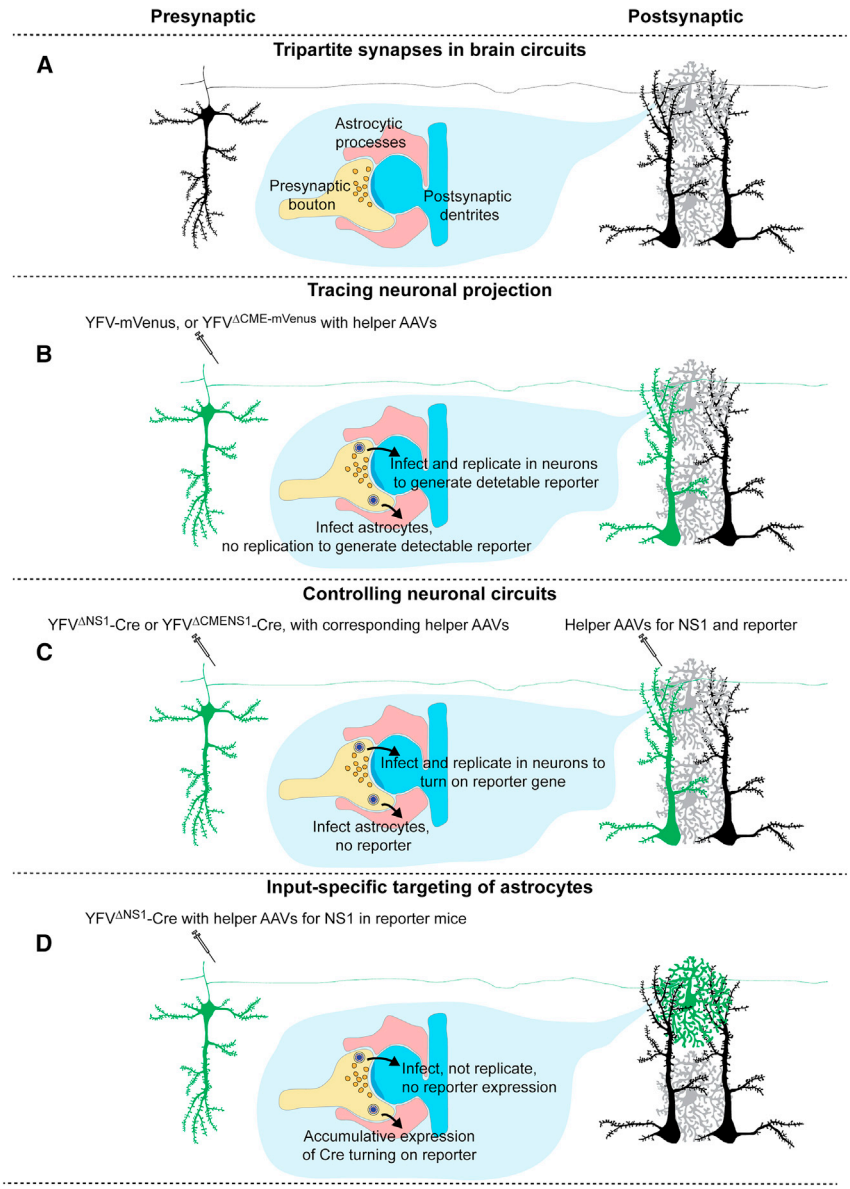

Figure 7. Different experimental schemes for tracing postsynaptic neurons or astrocytes

(A) Astrocytic processes enwrap neuron-neuron connection to form tripartite synapses.

(B) When replication-capable YFV-mVenus or YFV$^{\Delta CME}$-mVenus (with helper AAVs to express complementary genes, C-prM-E) is injected into a presynaptic region, it spreads to and infects postsynaptic neurons as well as astrocytes. In postsynaptic neurons, it replicates to express mVenus to a detectable level, whereas in astrocytes, it cannot generate detectable mVenus due to the lack of viral replication.

(C) When replication-incompetent YFV$^{\Delta NS1}$-Cre or YFV$^{\Delta CMENS1}$-Cre is injected into a presynaptic region, with helper AAVs expressing NS1 injected into both pre- and postsynaptic regions, both postsynaptic neurons and astrocytes are infected. In neurons, NS1 enables YFV$^{\Delta NS1}$-Cre or YFV$^{\Delta CMENS1}$-Cre to replicate and express Cre to a high level to turn on an AAV reporter. Because the reporter gene in the reporter AAV is controlled by a neuronal promoter, the reporter gene is not expressed in astrocytes.

(D) When the replication-incompetent YFV$^{\Delta NS1}$-Cre and helper AAVs expressing NS1 are injected into a presynaptic region in reporter mice, YFV$^{\Delta NS1}$-Cre infects both postsynaptic neurons and astrocytes. In postsynaptic neurons, due to the lack of NS1 it cannot replicate to express sufficient Cre. However, astrocytes, due to the large number of synapses with which they are associated, can accumulate multiple copies of YFV$^{\Delta NS1}$-Cre viral RNAs and express sufficient Cre to turn on the reporter gene under a ubiquitous promoter.

optimize the interval between the two injections and the dosage/timing of Dox to shorten the duration of the whole experiment and achieve a desirable level of labeling of astrocytes. In the future, we may even test self-complementary AAV vectors for expressing NS1. Self-complementary AAV vectors can initiate the expression of the gene it carries (such as NS1) quickly after infection,[62] which may allow us to inject the helper AAVs and YFV$^{\Delta NS1}$-Cre simultaneously in one mixture. Second, this tool traces astrocytes "monosynaptically" associated with the starter neurons, but brain functions are mediated by polysynaptic pathways. By optimizing the viral injection scheme, it is possible to trace the astrocytes associated with the second or third order of neurons connected with the starter neurons if we further provide NS1 in these downstream neurons. Third, we have been unable to efficiently turn on reporter genes carried by locally injected AAV under astrocyte-specific promoter. This is likely due to the defense mechanisms of astrocytes triggered by AAV infection. Potential solutions include shortening or elongating the time window between reporter AAV injection and YFV$^{\Delta NS1}$-Cre injection (shortening the interval may allow YFV$^{\Delta NS1}$-Cre to infect the astrocytes before the defense mechanisms kick in; elongating the interval may allow the defense mechanisms to subside by the time YFV$^{\Delta NS1}$-Cre infects the astrocytes) or pharmacological inhibition of cellular antiviral machinery. AAV reporters under astrocyte-specific promoters can be a convenient alternative to reporter mouse lines and allow this tool to be used in species other than mice. These optimizations will further broaden the applications of this method.

STAR★METHODS

Detailed methods are provided in the online version of this paper and include the following:

- KEY RESOURCES TABLE

SUPPLEMENTAL INFORMATION

Supplemental information can be found online at https://doi.org/10.1016/j.crmeth.2023.100653.

ACKNOWLEDGMENTS

We thank Elizabeth Li, Jun Guo, Heankel Oliveros, and So Jung Oh for their contributions at the early stage of this project. This project was supported by a grant from NIH/NIMH (1RF1MH130422 to W.X.). We also thank Dr. Denise Ramirez (Whole Brain Microscopy Facility at UT Southwestern) and Dr. Shin Yamazaki (Neuroscience Microscopy Facility at UT Southwestern) for their help with imaging.

AUTHOR CONTRIBUTIONS

W.X. designed and supervised this study. A.T., R.A., U.S., R.P., L.M., I.N., K.R., Y.K., Y.L., and W.X. generated viral vectors, conducted the experiments, and collected the data. W.X. and Y.L. plotted the figures and wrote the paper. All authors provided comments and suggestions on the manuscript.

DECLARATION OF INTERESTS

The authors declare no competing interests.

INCLUSION AND DIVERSITY

One or more of the authors of this paper self-identifies as an underrepresented ethnic minority in their field of research or within their geographical location. One or more of the authors of this paper self-identifies as a gender minority in their field of research.

Received: December 29, 2022
Revised: October 4, 2023
Accepted: November 8, 2023
Published: December 4, 2023

REFERENCES

1. Chai, H., Diaz-Castro, B., Shigetomi, E., Monte, E., Octeau, J.C., Yu, X., Cohn, W., Rajendran, P.S., Vondriska, T.M., Whitelegge, J.P., et al. (2017). Neural Circuit-Specialized Astrocytes: Transcriptomic, Proteomic, Morphological, and Functional Evidence. Neuron *95*, 531–549.e9.
2. Xu-Friedman, M.A., Harris, K.M., and Regehr, W.G. (2001). Three-dimensional comparison of ultrastructural characteristics at depressing and facilitating synapses onto cerebellar Purkinje cells. J. Neurosci. *21*, 6666–6672.
3. Farhy-Tselnicker, I., and Allen, N.J. (2018). Astrocytes, neurons, synapses: a tripartite view on cortical circuit development. Neural Dev. *13*, 7.
4. Stogsdill, J.A., Ramirez, J., Liu, D., Kim, Y.H., Baldwin, K.T., Enustun, E., Ejikeme, T., Ji, R.R., and Eroglu, C. (2017). Astrocytic neuroligins control astrocyte morphogenesis and synaptogenesis. Nature *551*, 192–197.
5. Ribot, J., Breton, R., Calvo, C.F., Moulard, J., Ezan, P., Zapata, J., Samama, K., Moreau, M., Bemelmans, A.P., Sabatet, V., et al. (2021). Astrocytes close the mouse critical period for visual plasticity. Science *373*, 77–81.
6. Perea, G., and Araque, A. (2005). Properties of synaptically evoked astrocyte calcium signal reveal synaptic information processing by astrocytes. J. Neurosci. *25*, 2192–2203.
7. Perea, G., Navarrete, M., and Araque, A. (2009). Tripartite synapses: astrocytes process and control synaptic information. Trends Neurosci. *32*, 421–431.
8. Deemyad, T., Lüthi, J., and Spruston, N. (2018). Astrocytes integrate and drive action potential firing in inhibitory subnetworks. Nat. Commun. *9*, 4336.
9. Savtchouk, I., and Volterra, A. (2018). Gliotransmission: Beyond Black-and-White. J. Neurosci. *38*, 14–25.
10. Hill, S.A., Blaeser, A.S., Coley, A.A., Xie, Y., Shepard, K.A., Harwell, C.C., Gao, W.J., and Garcia, A.D.R. (2019). Sonic hedgehog signaling in astrocytes mediates cell type-specific synaptic organization. Elife *8*, e45545.
11. Armbruster, M., Naskar, S., Garcia, J.P., Sommer, M., Kim, E., Adam, Y., Haydon, P.G., Boyden, E.S., Cohen, A.E., and Dulla, C.G. (2022). Neuronal activity drives pathway-specific depolarization of peripheral astrocyte processes. Nat. Neurosci. *25*, 607–616.
12. Semyanov, A., Henneberger, C., and Agarwal, A. (2020). Making sense of astrocytic calcium signals - from acquisition to interpretation. Nat. Rev. Neurosci. *21*, 551–564.
13. Schober, A.L., Wicki-Stordeur, L.E., Murai, K.K., and Swayne, L.A. (2022). Foundations and implications of astrocyte heterogeneity during brain development and disease. Trends Neurosci. *45*, 692–703.
14. Ben Haim, L., and Rowitch, D.H. (2017). Functional diversity of astrocytes in neural circuit regulation. Nat. Rev. Neurosci. *18*, 31–41.
15. Khakh, B.S., and Sofroniew, M.V. (2015). Diversity of astrocyte functions and phenotypes in neural circuits. Nat. Neurosci. *18*, 942–952.
16. Hasel, P., Rose, I.V.L., Sadick, J.S., Kim, R.D., and Liddelow, S.A. (2021). Neuroinflammatory astrocyte subtypes in the mouse brain. Nat. Neurosci. *24*, 1475–1487.
17. Bandler, R.C., Vitali, I., Delgado, R.N., Ho, M.C., Dvoretskova, E., Ibarra Molinas, J.S., Frazel, P.W., Mohammadkhani, M., Machold, R., Maedler, S., et al. (2022). Single-cell delineation of lineage and genetic identity in the mouse brain. Nature *601*, 404–409.
18. Gomez, J.A., Perkins, J.M., Beaudoin, G.M., Cook, N.B., Quraishi, S.A., Szoeke, E.A., Thangamani, K., Tschumi, C.W., Wanat, M.J., Maroof, A.M., et al. (2019). Ventral tegmental area astrocytes orchestrate avoidance and approach behavior. Nat. Commun. *10*, 1455.
19. Martin-Fernandez, M., Jamison, S., Robin, L.M., Zhao, Z., Martin, E.D., Aguilar, J., Benneyworth, M.A., Marsicano, G., and Araque, A. (2017). Synapse-specific astrocyte gating of amygdala-related behavior. Nat. Neurosci. *20*, 1540–1548.
20. Martín, R., Bajo-Grañeras, R., Moratalla, R., Perea, G., and Araque, A. (2015). Circuit-specific signaling in astrocyte-neuron networks in basal ganglia pathways. Science *349*, 730–734.
21. Oliveira, J.F., Sardinha, V.M., Guerra-Gomes, S., Araque, A., and Sousa, N. (2015). Do stars govern our actions? Astrocyte involvement in rodent behavior. Trends Neurosci. *38*, 535–549.
22. Georgiou, L., Echeverría, A., Georgiou, A., and Kuhn, B. (2022). Ca(+) activity maps of astrocytes tagged by axoastrocytic AAV transfer. Sci. Adv. *8*, eabe5371.
23. Wang, J., and Zhang, L. (2021). Retrograde axonal transport property of adeno-associated virus and its possible application in future. Microb. Infect. *23*, 104829.

24. Hollis Ii, E.R., Kadoya, K., Hirsch, M., Samulski, R.J., and Tuszynski, M.H. (2008). Efficient retrograde neuronal transduction utilizing self-complementary AAV1. Mol. Ther. *16*, 296–301.

25. Hadaczek, P., Stanek, L., Ciesielska, A., Sudhakar, V., Samaranch, L., Pivirotto, P., Bringas, J., O'Riordan, C., Mastis, B., San Sebastian, W., et al. (2016). Widespread AAV1- and AAV2-mediated transgene expression in the nonhuman primate brain: implications for Huntington's disease. Mol. Ther. Methods Clin. Dev. *3*, 16037.

26. Li, E., Guo, J., Oh, S.J., Luo, Y., Oliveros, H.C., Du, W., Arano, R., Kim, Y., Chen, Y.T., Eitson, J., et al. (2021). Anterograde transneuronal tracing and genetic control with engineered yellow fever vaccine YFV-17D. Nat. Methods *18*, 1542–1551.

27. Madisen, L., Zwingman, T.A., Sunkin, S.M., Oh, S.W., Zariwala, H.A., Gu, H., Ng, L.L., Palmiter, R.D., Hawrylycz, M.J., Jones, A.R., et al. (2010). A robust and high-throughput Cre reporting and characterization system for the whole mouse brain. Nat. Neurosci. *13*, 133–140.

28. Jeong, M., Kim, Y., Kim, J., Ferrante, D.D., Mitra, P.P., Osten, P., and Kim, D. (2016). Comparative three-dimensional connectome map of motor cortical projections in the mouse brain. Sci. Rep. *6*, 20072.

29. Torres-Ceja, B., and Olsen, M.L. (2022). A closer look at astrocyte morphology: Development, heterogeneity, and plasticity at astrocyte leaflets. Curr. Opin. Neurobiol. *74*, 102550.

30. Khakh, B.S. (2019). Astrocyte-Neuron Interactions in the Striatum: Insights on Identity, Form, and Function. Trends Neurosci. *42*, 617–630.

31. Minge, D., Domingos, C., Unichenko, P., Behringer, C., Pauletti, A., Anders, S., Herde, M.K., Delekate, A., Gulakova, P., Schoch, S., et al. (2021). Heterogeneity and Development of Fine Astrocyte Morphology Captured by Diffraction-Limited Microscopy. Front. Cell. Neurosci. *15*, 669280.

32. Lanjakornsiripan, D., Pior, B.J., Kawaguchi, D., Furutachi, S., Tahara, T., Katsuyama, Y., Suzuki, Y., Fukazawa, Y., and Gotoh, Y. (2018). Layer-specific morphological and molecular differences in neocortical astrocytes and their dependence on neuronal layers. Nat. Commun. *9*, 1623.

33. Hösli, L., Zuend, M., Bredell, G., Zanker, H.S., Porto de Oliveira, C.E., Saab, A.S., and Weber, B. (2022). Direct vascular contact is a hallmark of cerebral astrocytes. Cell Rep. *39*, 110599.

34. Liljeholm, M., and O'Doherty, J.P. (2012). Contributions of the striatum to learning, motivation, and performance: an associative account. Trends Cognit. Sci. *16*, 467–475.

35. Dimidschstein, J., Chen, Q., Tremblay, R., Rogers, S.L., Saldi, G.A., Guo, L., Xu, Q., Liu, R., Lu, C., Chu, J., et al. (2016). A viral strategy for targeting and manipulating interneurons across vertebrate species. Nat. Neurosci. *19*, 1743–1749.

36. Risold, P.Y., and Swanson, L.W. (1997). Chemoarchitecture of the rat lateral septal nucleus. Brain Res. Brain Res. Rev. *24*, 91–113.

37. Lin, W., McKinney, K., Liu, L., Lakhlani, S., and Jennes, L. (2003). Distribution of vesicular glutamate transporter-2 messenger ribonucleic Acid and protein in the septum-hypothalamus of the rat. Endocrinology *144*, 662–670.

38. Chen, Y.T., Arano, R., Guo, J., Saleem, U., Li, Y., and Xu, W. (2023). Inhibitory hippocampus-medial septum projection controls locomotion and exploratory behavior. Front. Synaptic Neurosci. *15*, 1042858.

39. Liddelow, S.A., and Barres, B.A. (2017). Reactive Astrocytes: Production, Function, and Therapeutic Potential. Immunity *46*, 957–967.

40. Ortinski, P.I., Dong, J., Mungenast, A., Yue, C., Takano, H., Watson, D.J., Haydon, P.G., and Coulter, D.A. (2010). Selective induction of astrocytic gliosis generates deficits in neuronal inhibition. Nat. Neurosci. *13*, 584–591.

41. Yu, X., Taylor, A.M.W., Nagai, J., Golshani, P., Evans, C.J., Coppola, G., and Khakh, B.S. (2018). Reducing Astrocyte Calcium Signaling In Vivo Alters Striatal Microcircuits and Causes Repetitive Behavior. Neuron *99*, 1170–1187.e9.

42. Santello, M., Toni, N., and Volterra, A. (2019). Astrocyte function from information processing to cognition and cognitive impairment. Nat. Neurosci. *22*, 154–166.

43. Lee, H.G., Wheeler, M.A., and Quintana, F.J. (2022). Function and therapeutic value of astrocytes in neurological diseases. Nat. Rev. Drug Discov. *21*, 339–358.

44. Petrelli, F., Pucci, L., and Bezzi, P. (2016). Astrocytes and Microglia and Their Potential Link with Autism Spectrum Disorders. Front. Cell. Neurosci. *10*, 21.

45. González-Reyes, R.E., Nava-Mesa, M.O., Vargas-Sánchez, K., Ariza-Salamanca, D., and Mora-Muñoz, L. (2017). Involvement of Astrocytes in Alzheimer's Disease from a Neuroinflammatory and Oxidative Stress Perspective. Front. Mol. Neurosci. *10*, 427.

46. Izrael, M., Slutsky, S.G., and Revel, M. (2020). Rising Stars: Astrocytes as a Therapeutic Target for ALS Disease. Front. Neurosci. *14*, 824.

47. Coulter, D.A., and Steinhäuser, C. (2015). Role of astrocytes in epilepsy. Cold Spring Harb. Perspect. Med. *5*, a022434.

48. Lindqvist, R., Mundt, F., Gilthorpe, J.D., Wölfel, S., Gekara, N.O., Kröger, A., and Överby, A.K. (2016). Fast type I interferon response protects astrocytes from flavivirus infection and virus-induced cytopathic effects. J. Neuroinflammation *13*, 277.

49. Bushong, E.A., Martone, M.E., Jones, Y.Z., and Ellisman, M.H. (2002). Protoplasmic astrocytes in CA1 stratum radiatum occupy separate anatomical domains. J. Neurosci. *22*, 183–192.

50. Callaway, E.M., and Luo, L. (2015). Monosynaptic Circuit Tracing with Glycoprotein-Deleted Rabies Viruses. J. Neurosci. *35*, 8979–8985.

51. Wickersham, I.R., Lyon, D.C., Barnard, R.J.O., Mori, T., Finke, S., Conzelmann, K.K., Young, J.A.T., and Callaway, E.M. (2007). Monosynaptic restriction of transsynaptic tracing from single, genetically targeted neurons. Neuron *53*, 639–647.

52. Pfefferkorn, C., Kallfass, C., Lienenklaus, S., Spanier, J., Kalinke, U., Rieder, M., Conzelmann, K.K., Michiels, T., and Staeheli, P. (2016). Abortively Infected Astrocytes Appear To Represent the Main Source of Interferon Beta in the Virus-Infected Brain. J. Virol. *90*, 2031–2038.

53. Clark, I.C., Gutiérrez-Vázquez, C., Wheeler, M.A., Li, Z., Rothhammer, V., Linnerbauer, M., Sanmarco, L.M., Guo, L., Blain, M., Zandee, S.E.J., et al. (2021). Barcoded viral tracing of single-cell interactions in central nervous system inflammation. Science *372*, eabf1230.

54. Card, J.P., Rinaman, L., Schwaber, J.S., Miselis, R.R., Whealy, M.E., Robbins, A.K., and Enquist, L.W. (1990). Neurotropic properties of pseudorabies virus: uptake and transneuronal passage in the rat central nervous system. J. Neurosci. *10*, 1974–1994.

55. Card, J.P., Rinaman, L., Lynn, R.B., Lee, B.H., Meade, R.P., Miselis, R.R., and Enquist, L.W. (1993). Pseudorabies virus infection of the rat central nervous system: ultrastructural characterization of viral replication, transport, and pathogenesis. J. Neurosci. *13*, 2515–2539.

56. McCarthy, M., Norenberg, M.D., Norenberg, L.O., and Dix, R.D. (1990). Herpes simplex virus type 1 infection of rat astrocytes in primary culture: effects of dibutyryl cyclic AMP. J. Neuropathol. Exp. Neurol. *49*, 3–20.

57. Ugolini, G., Kuypers, H.G., and Simmons, A. (1987). Retrograde transneuronal transfer of herpes simplex virus type 1 (HSV 1) from motoneurones. Brain Res. *422*, 242–256.

58. Rogers, A., and Beier, K.T. (2021). Can transsynaptic viral strategies be used to reveal functional aspects of neural circuitry? J. Neurosci. Methods *348*, 109005.

59. Rinaman, L., Card, J.P., and Enquist, L.W. (1993). Spatiotemporal responses of astrocytes, ramified microglia, and brain macrophages to central neuronal infection with pseudorabies virus. J. Neurosci. *13*, 685–702.

60. Daigle, T.L., Madisen, L., Hage, T.A., Valley, M.T., Knoblich, U., Larsen, R.S., Takeno, M.M., Huang, L., Gu, H., Larsen, R., et al. (2018). A Suite

of Transgenic Driver and Reporter Mouse Lines with Enhanced Brain-Cell-Type Targeting and Functionality. Cell *174*, 465–480.e22.

61. Zhu, H., Aryal, D.K., Olsen, R.H.J., Urban, D.J., Swearingen, A., Forbes, S., Roth, B.L., and Hochgeschwender, U. (2016). Cre-dependent DREADD (Designer Receptors Exclusively Activated by Designer Drugs) mice. Genesis *54*, 439–446.
62. McCarty, D.M. (2008). Self-complementary AAV vectors; advances and applications. Mol. Ther. *16*, 1648–1656.
63. Zolotukhin, S., Byrne, B.J., Mason, E., Zolotukhin, I., Potter, M., Chesnut, K., Summerford, C., Samulski, R.J., and Muzyczka, N. (1999). Recombinant adeno-associated virus purification using novel methods improves infectious titer and yield. Gene Ther. *6*, 973–985.

CellPress
OPEN ACCESS

STAR★METHODS

KEY RESOURCES TABLE

REAGENT or RESOURCE	SOURCE	IDENTIFIER
Antibodies		
NeuN	Sigma	Cat# MAB377; RRID:AB_2298772
S100β	AbCam	Cat# ab41548; RRID:AB_956280
Olig2	Sigma	Cat# MABN50; RRID:AB_10807410
NG2	Sigma/Millipore	Cat# AB5320; RRID:AB_91789
TMEM119	AbCam	Cat# ab209064; RRID:AB_280034
GFAP	Cell Signaling	Cat# 12389; RRID:AB_2631098
Alexa Fluor 594- or Alexa Fluor 488-onjugated Secondary Antibodies	ThermoFisher	Cat# A-11032; RRID:AB_2534091, Cat# A-11034; RRID: AB_2576217. Cat# A28175; RRID: AB_2536161
Bacterial and virus strains		
AAV-Syn-tTA	Li, E. et al.[26]	Addgene 175280
AAV-TRE-NS1	Li, E. et al.[26]	Addgene 175279
AAV-Dlx-tTA	This paper	GenBank Accession #: OR725555; Addgene 210730
AAV-CamK2-tTA	This paper	GenBank Accession #: OR725557; Addegene 210731
YFV$^{\Delta NS1}$-Cre	Li, E. et al.[26]	Addgene 179952
YFV$^{\Delta CME}$-mVenus	Li, E. et al.[26]	Addgene 179953
pAAV-Syn-SynaptoTAG2	Li, E. et al.[26]	Addgene 175275
pAAV-Dlx-SynaptoTAG	Chen et al.[38]	GenBank Accession #: OR725556, Addgene 210729
AAV1-Cre	N/A	Addgene, 105545-AAV1
Chemicals, peptides, and recombinant proteins		
Doxycycline hyclate food	Inotiv	TD.01306
Paraformaldehyde (PFA)	Electron Microscopy Sciences	19210
Deposited data		
The raw data of microscopic images of brain sections and data used to plot the graphs	This paper	https://doi.org/10.5281/zenodo.10019905
Experimental models: Cell lines		
HEK293T cell	ATCC	CRL-3216
BHK-21 cells	ATCC	CCL-10
Experimental models: Organisms/strains		
Mouse: C57BL/6J	The Jackson Laboratory	000664
Mouse: Ai9	The Jackson Laboratory	007909
Mouse: Ai6	The Jackson Laboratory	007906
Mouse: Calb2-Cre	The Jackson Laboratory	010774

RESOURCE AVAILABILITY

Lead contact

Further information and requests for resources and reagents should be directed to the lead contact, Wei Xu (wei.xu1@utsouthwestern.edu).

Materials availability

The AAV plasmids generated in this study, pAAV-CamK2-tTA and pAAV-Dlx-tTA, are deposited to Addgene. The sequences are deposited to GenBank. The plasmid IDs and accession numbers are listed in the key resources table. Other reagents reported in this paper are available from the lead contact upon request.

Data and code availability

- The raw data of microscopic images of brain sections are deposited to Zenodo and will be publicly available as of the date of publication. The DOI is listed in the key resources table. All data reported in this paper will also be shared by the lead contact upon request.
- This paper does not report original code.
- Any additional information required to reanalyze the data reported in this paper is available from the lead contact upon request.

EXPERIMENTAL MODEL AND STUDY PARTICIPANT DETAILS

Mice

6-24 weeks old male and female C57BL/6J mice (JAX# 000664), tdTomato reporter mice (Ai9 mice, JAX# 007909) and ZsGreen1 reporter mice (Ai6 mice, JAX# 007906), and Calb2-Cre mice (JAX# 010774) were group housed on a 12 h light/12 h dark cycle with *ad libitum* access to food and water. Since our previous work does not show a difference of animals' sex in YFV-17D tracing, the sex of the mice was not accounted for in this study. Male and female mice were randomly assigned to experimental groups. Animal work was approved by and conducted under the oversight of the UT Southwestern Institutional Animal Care and Use Committee and complied with Guide for the Care and Use of Laboratory Animals by National Research Council.

Cell culture

293T cells and BHK cells were used to generate AAV, $YFV^{\Delta NS1}$-Cre (or $YFV^{\Delta CME}$-mVenus), respectively. 293T and BHK cells were grown in Dulbecco's Modified Eagle's Medium (DMEM) containing 10% Fetal Bovine Serum (FBS).

METHOD DETAILS

Preparation of viral vectors

The helper AAVs (AAV-Syn-tTA, AV-CamK2-tTA and AAV-Dlx-tTA) were packaged with AAV-DJ capsids.[63] AAV5-GfaABC1D-DIO-SypminiSOG2-mCherry was packaged with AAV5 capsids. Briefly, AAV vectors were co-transfected with pHelper and pRC-DJ into AAV-293 cells. Cells were collected 72 h later, lysed, and loaded onto iodixanol gradient for centrifugation at 400,000 g for 2 h. The fraction with 40% iodixanol of the gradient was collected, washed, and concentrated with 100,000 MWCO tube filter. The genomic titer of virus was measured with quantitative real-time PCR (qRT-PCR). The titers of AAVs used for stereotaxic injection were in the range of 1–2 x 10^{13} genome copies/ml. To generate YFV-17D stocks, plasmids were linearized with XhoI digestion and transcribed with an SP6 *in vitro* transcription kit (mMESSAGE mMACHINE Kit, Ambion). *In vitro* transcribed viral RNAs, generated from linearized plasmids encoding $YFV^{\Delta NS1}$-Cre, was transfected into BHK cells (ATCC CCL-10) with TransIT-mRNA Transfection Kit (Mirus Bio, Cat.# MIR 2225). Virus containing supernatant was concentrated, aliquoted, stored at −80C, and tittered by qRT-PCR. The titer of $YFV^{\Delta NS1}$-Cre was 9.60X10^{10} genome copies/ml; the titer of $YFV^{\Delta CME}$-mVenus was 3.12X10^{11} genome copies/ml.

Stereotaxic injections

Mice were anesthetized with isoflurane inhalation (1.5–2%). Viral solution was injected with a glass pipette at a flow rate of 0.10 μL/min. After the completion of injection, the glass pipette was left in place for 5 min before being retrieved slowly. We unilaterally injected 0.50–0.75 μL of viral solution at each injection site unless stated otherwise. The coordinates for each of the injection sites on the anterior-posterior direction from the bregma (AP), medial-lateral direction from the midline, and the dorsal-ventral direction from the dura (DV) are as the following: Mo (+0.50, 1.50. 0.80), PFC (+1.25, 0.30, 1.25); LEC (−3.20, 4.60, 3.60); MEC (−4.80, 3.45, 2.75); LS (+0.55, 0.45, 2.70) (In the AP direction, "+" denotes anterior to the bregma and "-" denotes posterior to bregma).

Histology and immunohistochemistry

Mice were transcardially perfused with 10 mL of PBS followed by 30–40 mL of 4% paraformaldehyde (PFA) in PBS. The brains were extracted and postfixed overnight in 4% PFA at 4°C, and cryoprotected in 30% sucrose. Brains were sectioned with a cryostat to a thickness of 30 or 40-μm. Free-floating sections were washed in PBS, incubated with DAPI (1 μg/ml) and mounted on slides. For immunohistochemistry, the brain sections were washed in PBS three times and permeabilized in 2% Triton X-100 in PBS for 2 h. The sections were then incubated for 2 h in PBS containing 10% horse serum, 0.2% bovine serum albumin and 0.5% Triton X-100, followed by overnight incubation in a primary antibody diluted in PBS containing 1% horse serum and 0.2% bovine serum albumin. The primary antibodies and their dilutions are: NeuN antibody (clone A60), Sigma MAB377, 1:1,000; S100β antibody, AbCam ab41548, 1:500; Olig2 antibody, Sigma MABN50, 1:200; TMEM119 antibody, AbCam ab209064, 1:500; NG2 antibody, Sigma/Millipore AB5320, 1:500; GFAP antibody, Cell Signaling 12389, 1:1000. After three washes in PBS, the sections were then incubated

in the secondary antibody for 2 h, washed again and then mounted onto glass slides. The secondary antibodies and their dilutions are Alexa Fluor 488- or Alexa Fluor 594-conjugated goat anti-mouse or goat anti-rabbit IgG (Thermo Fisher) 1:500. The whole-mount brain sections were tile scanned with Zeiss AxioscanZ1 digital slide scanner with a 10X objective. The high-resolution images were taken with ZEISS LSM 880 confocal microscope. The intensity of fluorescence of GFAP immunostaining, the intensity of native green fluorescence of EGFP (of SynaptoTAG2, without immunostaining), and areas of the regions of interest were measured with Zen software (Carl Zeiss Microscopy GmbH). The number of tdTomato-positive cells or the cells immunostained with antibodies (for S100β, Olig2, NeuN, NG2, TMEM119, respectively) were manually counted. The density of positive cells (expressing tdTomato, or immunostained with antibodies) was calculated by dividing the cell number by the area of the brain region.

QUANTIFICATION AND STATISTICAL ANALYSIS

Data are presented as scatter and mean, or mean ± standard error of the mean (SEM). Sample numbers (n) indicating the number of brain images in each experiment are specified in the figures. The correlation between the densities of astrocytes and intensity of EGFP-Syb2 (of SynaptoTAG2) in Figure 1 is conducted with linear regression. Statistical significance was analyzed with Mann-Whitney test. $p < 0.05$ is considered statistically significant. "****" in the figures indicates $p < 0.001$.